Journal of Power Sources 273 (2015) 396–403

Contents lists available at ScienceDirect

Journal of Power Sources

journal homepage: www.elsevier.com/locate/jpowsour

Synthesis and electrochemical properties of novel $LiFeTiO_4$ and Li_2FeTiO_4 polymorphs with the $CaFe_2O_4$-type structures

Shaun R. Bruno [a], Colin K. Blakely [a], Jonathon B. Clapham [a], Joshua D. Davis [a], Wenli Bi [b, c], E. Ercan Alp [b], Viktor V. Poltavets [a, *]

[a] Department of Chemistry, Michigan State University, East Lansing, MI 48824, USA
[b] Advanced Photon Source, Argonne National Laboratory, Argonne, IL 60439, USA
[c] Department of Geology, University of Illinois at Urbana-Champaign, Urbana, IL 61801, USA

HIGHLIGHTS

- New $LiFeTiO_4$ polymorph with the $CaFe_2O_4$-type structure was prepared via ion exchange.
- Li deintercalation leads to decomposition without Fe^{4+} formation.
- Li intercalation preserves the structural motif and results in Li_2FeTiO_4 compound.
- $LiFeTiO_4$ electrochemical cycling vs. Li occurs between 2 and 2.3 V.
- Li^+ bond valence sum maps indicate high ionic conductivity in the compounds.

GRAPHICAL ABSTRACT

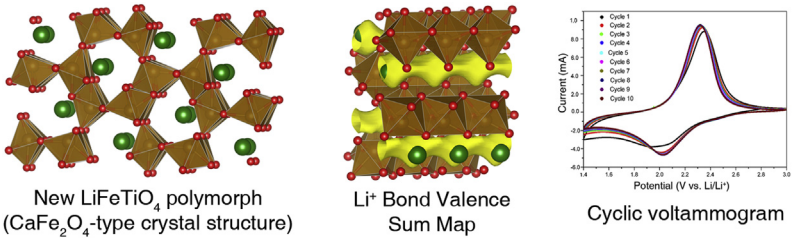

ARTICLE INFO

Article history:
Received 1 July 2014
Received in revised form
17 September 2014
Accepted 18 September 2014
Available online 28 September 2014

Keywords:
Lithium-ion batteries
Cathode
Crystal structure
$LiFeTiO_4$ polymorph

ABSTRACT

The new $LiFeTiO_4$ polymorph with the $CaFe_2O_4$-type (CF) crystal structure was synthesized via ion exchange from $NaFeTiO_4$. Due to the presence of tunnels sufficiently large to accommodate additional Li^+ ions, CF-$LiFeTiO_4$ was studied as a model compound for potential cathode material utilizing Fe^{2+}/Fe^{3+} (on Li intercalation) as well as Fe^{3+}/Fe^{4+} (on Li deintercalation) redox couples. Chemical and electrochemical Li intercalation preserves the structural motif of CF-$LiFeTiO_4$ and results in Li_2FeTiO_4 compound. The electrochemical cycling of CF-$LiFeTiO_4$ vs. Li occurs between 2 and 2.3 V with an initial specific capacity of 148 mAh g^{-1}. High Li^+ ionic conductivity in the compound is suggested based on the interconnection of Li^+ bond valence sum isosurfaces at a bond valence sum value of 1.0. Chemical Li deintercalation from CF-$LiFeTiO_4$ results in compound decomposition without Fe^{4+} formation, as confirmed by Mössbauer spectroscopy.

1. Introduction

The discovery of novel materials for rechargeable lithium ion batteries played a pivotal role in the advancement of modern day technologies, providing high energy density batteries for portable electronics and electric vehicles. Due to concerns over toxicity and the high cost of Co in $LiCoO_2$, many researchers focused on search for cathodes with inexpensive and less toxic transition metals such as Mn, Ni, and Fe [1,2]. $LiFePO_4$, which crystallizes in the olivine structure type, was proposed by Goodenough's research group in 1997 [3]. Electrochemical properties of many other cathodes utilizing Fe^{2+}/Fe^{3+} redox couple were investigated: Fe_2O_3 [4–10], Fe_3O_4 [5], $LiFePO_4$ [3,11–13], FeOOH [14–22], tetrahedral $LiFeO_2$

* Corresponding author. Tel.: +1 517 355 9718x388; fax: +1 517 353 1793.
E-mail addresses: poltavets@chemistry.msu.edu, victor@poltavets.com (V.V. Poltavets).

http://dx.doi.org/10.1016/j.jpowsour.2014.09.115
0378-7753/

[23], $FeBO_3$ [24], Fe_3BO_6 [24,25], $LiFeBO_3$ [26,27], $LiFeSO_4F$ [28], Li_2FePO_4F [29], Li_2FeSiO_4 [30]. However, electrochemical cycling of one Li per Fe atom imposes an intrinsic limit on the maximum possible cathode specific energy. To further increase the cathode energy density, intercalation materials that can transfer multiple electrons per transition metal ion are necessary. In such cathodes, the Fe^{2+}/Fe^{3+} as well as Fe^{3+}/Fe^{4+} redox couples will be utilized. While it is hard to stabilize Fe^{4+} in oxides, Mössbauer spectroscopy data confirmed Fe^{4+} formation by alkali ion deintercalation from $Li(Fe_yMn_{2-y})O_4$ [31] and $NaFeO_2$ [32]. Recently, cycling of more than one Li^+ per Li_2FeSiO_4 formula unit was demonstrated [33,34].

In this article, the synthesis, structure and electrochemical properties of a new $LiFeTiO_4$ polymorph with the $CaFe_2O_4$-type crystal structure (CF-$LiFeTiO_4$) is reported. CF-$LiFeTiO_4$ notation is used in the article to distinguished $CaFe_2O_4$-type structure from the known spinel polymorph. CF-$LiFeTiO_4$ was used as a model compound for a possible cathode with two electrons per Fe atom transfer. Li intercalation preserves the structural motif of CF-$LiFeTiO_4$ and results in the Li_2FeTiO_4 phase. Discussion of the crystal structure–property relationships for the new compounds with $CaFe_2O_4$-type structures is presented alongside a discussion of the known spinel, $LiFeTiO_4$ [35], and rock-salt, Li_2FeTiO_4 [36], polymorphs.

2. Experimental

2.1. Synthesis of $NaFeTiO_4$ and CF-$LiFeTiO_4$

All reagents used were of ACS grade purity or higher and were used without further purification. $LiNO_3$ (99%), Fe_2O_3 (99.5%), TiO_2 (99.5%), n-pentane (anhydrous 99.8%) and methanol (anhydrous 99.9%) were obtained from Alfa Aesar. Na_2CO_3 (99%) and acetonitrile (99.5%) were purchased from Mallinckrodt Chemicals. Bromine (99.5%) and iodine (99.8%) were obtained from Jade Scientific. N-butyllithium (2.5 M in hexanes) was purchased from Sigma–Aldrich.

For the preparation of $NaFeTiO_4$, stoichiometric ratios of Fe_2O_3, and TiO_2 were intimately mixed with a 5% molar excess of Na_2CO_3 using a planetary ball mill. Ball milling was performed for six cycles of five minutes at 500 rpm in steel mill jars using four tungsten carbide balls per jar. The mixture was then pelleted in a 3/4″ pellets at 5 tons pressure, placed in an alumina boat, annealed at 850 °C for 12 h in air, reground, and subjected to an additional heat treatment at 975 °C for 48 h in air.

The new $LiFeTiO_4$ polymorph with the $CaFe_2O_4$-type structure was synthesized via an ion exchange of Li^+ for Na^+ in $NaFeTiO_4$. For the CF-$LiFeTiO_4$ preparation, a twofold excess of $LiNO_3$ was intimately mixed with an equivalence of $NaFeTiO_4$ followed by thermal treatment at 325 °C for 48 h under O_2 flow. The $NaNO_3$ byproduct and excess $LiNO_3$ were washed out with anhydrous methanol utilizing a Soxhlet extractor. Following, the $LiFeTiO_4$ powder was dried under vacuum and stored under dry N_2 in a glovebox.

2.2. Chemical lithium intercalation and deintercalation

Chemical lithium deintercalation from CF-$LiFeTiO_4$ was performed for 48 h with stirring in a round bottom flask topped with 100 mL of acetonitrile utilizing double molar excess Br_2 or I_2 than stoichiometrically needed for complete Li removal. The reaction was carried out in a glove bag under dry N_2 atmosphere. The final product was filtered, washed with acetonitrile, dried under vacuum and stored under N_2 in a glovebox.

Lithium intercalation into CF-$LiFeTiO_4$ was performed in a nitrogen glovebox by reacting CF-$LiFeTiO_4$ with a 5% molar excess solution of n-butyllithium. The mixture was stirred at room temperature for 48 h, filtered, washed with pentane, dried under vacuum, and stored under N_2 in a glovebox.

2.3. Instrumentation and characterization

The samples were characterized by powder X-ray diffraction (PXD) on a Bruker D2-Phaser diffractometer using Cu K_α radiation. The diffractometer was located inside a dry N_2 purged glove box. The patterns were acquired at room temperature with a step size of 0.02° (2Θ) on a zero background sample holder. Rietveld refinement of the PXD data was performed with the GSAS software [37] with EXPGUI interface [38]. In the final Rietveld refinement runs the scale factor, unit-cell parameters, atomic coordinates, isotropic atomic displacement parameters, peak profiles, and background coefficients were simultaneously refined. Elemental composition was determined by inductively coupled plasma (ICP) spectroscopy using a Vista-MPX CCD Simultaneous ICP-OES instrument (Varian Inc.). Thermogravimetric analysis (TGA) was performed using a Netzsch STA 449 F3 Jupiter instrument.

Bond valence sum maps were calculated utilizing the BVS-Mapping code by Matthew Dyer from the University of Liverpool. VESTA software was used for structures and isosurfaces visualization [39].

Cyclic voltammetry (CV) experiments were carried out with two-electrode cells with a Li metal disc used as both counter and reference electrode. 19 mm discs of active material was prepared by ball milling a slurry consisting of 75% by weight of $LiFeTiO_4$, 10% by weight PTFE and 15% by weight Super C65 carbon (TIMCAL) in 1-methyl-2-pyrrolidone. The 30 micrometers thick slurry layer was deposited on aluminum foil using a doctor-blade technique. A 1 M solution of $LiPF_6$ in ethylene carbonate (EC), dimethyl carbonate (DMC) and diethyl carbonate (DEC) (EC/DMC/DEC = 1:1:1 ratio by volume) was used as the electrolyte. Electrochemical experiments were performed on a Reference 600 potentiostat (Gamry). All cells were assembled, sealed and tested under an Ar atmosphere in a glovebox.

Scanning Electron Microscopy (SEM) was performed using a JEOL JSM 6610LV. The sample was mounted on carbon tape under ambient conditions then gold coated. An accelerating voltage of 12 kV was used for all images acquired at different magnifications.

^{57}Fe Mössbauer spectroscopy was carried out utilizing a ^{57}Co-source in a Rh matrix at room temperature on polycrystalline powders pressed between two sheets of mylar film. All isomer shifts, δ, are given with respect to metallic α–Fe at room temperature. The measured spectrum was evaluated using Fit; o) – a Mössbauer spectrum fitting program [40].

3. Results and discussion

3.1. Target crystal structure selection

Several principles were used to identify a model structure for potential Fe^{2+}/Fe^{4+} cathode material for Li-ion batteries.

(1) The initial compound should contain Fe in the 3+ oxidation state to minimize structural stresses during Li^+ intercalation/deintercalation. Ease of synthesizing Fe^{3+} compounds in air is an advantage, which can eventually translate into lower manufacturing cost.
(2) Only tunnel structures were considered because they have been shown to be more stable at low Li content during electrochemical cycling.
(3) Uniquely, we considered only structures with tunnels sufficiently large to accommodate additional Li^+ ions, i.e. the initial structure need to contain larger Na^+ or K^+ cations

which can be exchanged for Li^+ using soft chemistry methods.

The calcium ferrite, $CaFe_2O_4$, tunnel structure (Fig. 1(a)) was chosen as a starting point to investigate whether a phase containing both Li and Fe with this structural type could be synthesized. Since no appropriate compounds were known, we pursued the synthesis of a new CF-$LiFeTiO_4$ polymorph with the $CaFe_2O_4$-type structure via the low temperature ion exchange reaction starting from $NaFeTiO_4$.

3.2. Synthesis

For the preparation of $NaFeTiO_4$ an annealing step at 850 °C was necessary to avoid melting of Na_2CO_3 at 851 °C. When the stoichiometric mixture of TiO_2, Fe_2O_3 and 10% excess of Na_2CO_3 was used, $NaFeTiO_4$ as well as small amount of α-$NaFeO_2$ admixture were formed after annealing in air at 850 °C for 12 h and at 975 °C for 48 h. Multiple intermittent grinding, pelleting and firing at 975 °C for long duration (~350 h) were necessary for the formation of pure $NaFeTiO_4$. When lower (5%) excess of Na_2CO_3 was used, the preparation time of $NaFeTiO_4$ decreased to 12 h at 850 °C and 48 h at 975 °C with just one intermittent grinding and pelleting. The PXD pattern of the prepared $NaFeTiO_4$ compound was matched to entry number 22209 from the Inorganic Crystal Structures Database (ICSD) and determined to be a pure phase sample (Fig. 2(a)). Initial attempts to synthesize $LiFeTiO_4$ through the ion exchange of Li^+ for Na^+ from $NaFeTiO_4$ at 250 °C under O_2 flow were unsuccessful. Upon increasing the temperature to 350 °C, successful ion exchange was observed after 48 h (determined by ICP analysis) resulting in a Li:Fe ratio of 1.00:1.00 with no sodium detection. The PXD pattern after the exchange at 350 °C contained peaks of the known $LiFeTiO_4$ spinel polymorph. Further attempts at the ion exchange at 300 °C for 250 h showed successful exchange with less intense peaks of the spinel structure. Decreasing the exchange time to 24 h at 300 °C showed partial exchange, while increasing the time to 72 h showed the formation of the spinel structure. Holding the exchange time to 48 h at 300 °C allowed the ion exchange to occur completely and without formation of the spinel polymorph (Fig. 2(b)). The following reaction has occurred:

$$NaFeTiO_4 + LiNO_3 \rightarrow \text{CF-}LiFeTiO_4 + NaNO_3\,. \quad (1)$$

As seen above, longer exchange times and temperatures higher than 300 °C clearly led to the transformation of the calcium ferrite type CF-$LiFeTiO_4$ to the spinel polymorph. Therefore, CF-$LiFeTiO_4$ is only kinetically stable and is unstable toward the transformation to the thermodynamically preferred spinel polymorph. This observation was further confirmed by TGA experiments. TGA-DSC measurements of CF-$LiFeTiO_4$ under O_2 or N_2 flow to a temperature of 1000 K were performed. The resulting sample was removed and analyzed by PXD, whereby it was determined that the CF-$LiFeTiO_4$ calcium ferrite structure transforms to the spinel structure under both O_2 and N_2 atmospheres (Fig. 2(d)). The TGA curves (Fig. 3) demonstrate mass losses of 0.38 and 1.11% under O_2 and N_2 flows which indicate oxygen deficiency in the formed $LiFeTiO_{4-x}$ spinel. The oxygen nonstoichiometry (x) values were 0.04 and 0.12 after TGA experiments under O_2 and N_2 flows respectively.

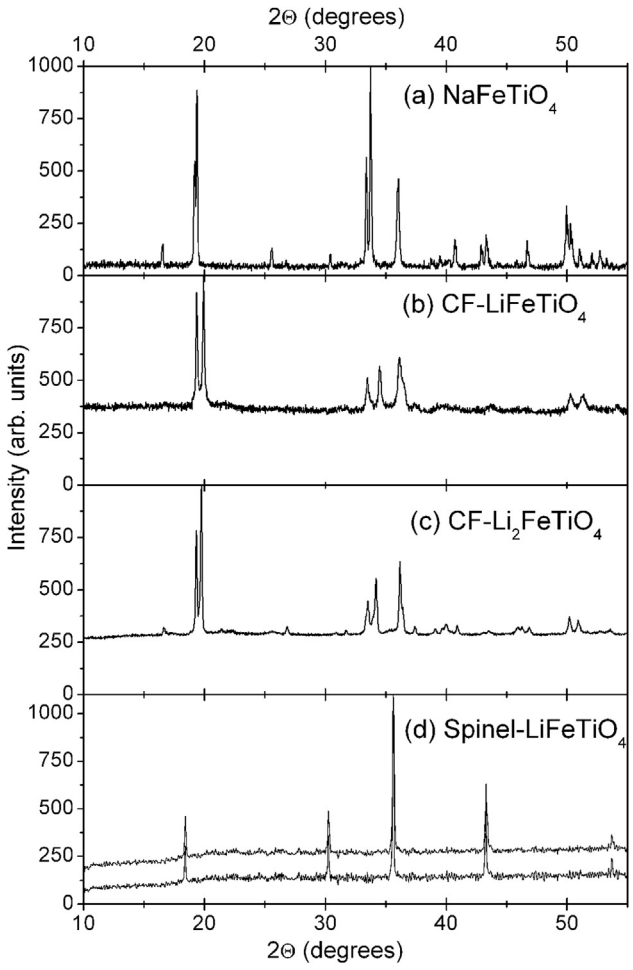

Fig. 2. Powder X-ray diffraction patterns for (a) $NaFeTiO_4$, (b) CF-$LiFeTiO_4$, (c) CF-Li_2FeTiO_4, and (d) spinel $LiFeTiO_4$ polymorph from CF-$LiFeTiO_4$ decomposition during a TGA measurement in O_2 (top pattern), and N_2 (bottom pattern) atmospheres. The "CF" label denotes $CaFe_2O_4$-type structures.

3.3. Morphology and particle size

Scanning electron microscopy was employed to determine the morphology and particle size of the as prepared CF-$LiFeTiO_4$. The particles (Fig. 4) were observed to have a size in the micrometer regime as expected with the high temperature synthetic procedure used for the parent $NaFeTiO_4$ phase. The morphology of the

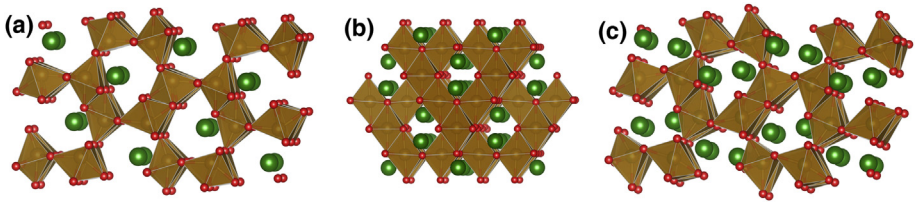

Fig. 1. Crystal structure models of (a) CF-$LiFeTiO_4$ ($CaFe_2O_4$-type structure), (b) $LiFeTiO_4$ in idealized spinel structure with Li/Fe mixing not shown, and (c) CF-Li_2FeTiO_4 ($CaFe_2O_4$-type structure). Li atoms are shown as green large spheres while small red balls represent O ions. FeO_6 octahedra are highlighted for clarity. (For interpretation of the references to color in this figure legend, the reader is referred to the web version of this article.)

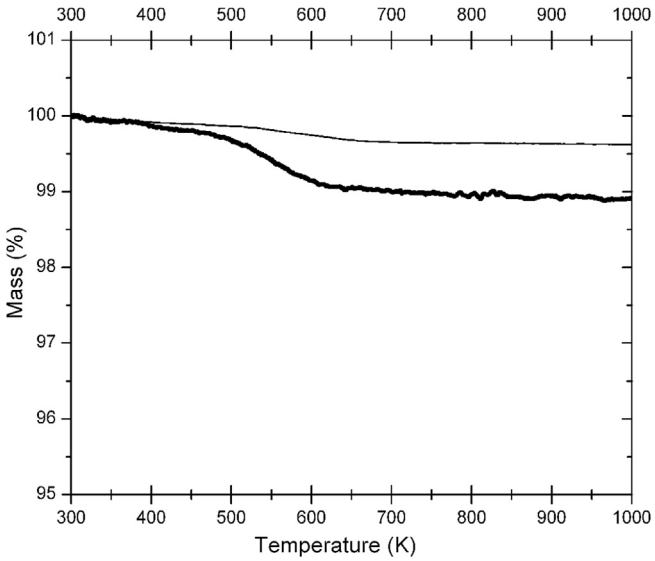

Fig. 3. Thermogravimetric studies of CF-$LiFeTiO_4$ in oxygen (thin line) and nitrogen (thick line) environments.

particles was generally rod-like. Smaller particles were observed on the surface of the $LiFeTiO_4$, possibly due to the presence of the $NaNO_3$ byproduct from the ion exchange reaction (1) which was not completely washed out in this particular synthetic batch.

3.4. Chemical lithium intercalation

Reduction via chemical lithium intercalation was initially attempted by the addition of solutions of 1, 5, and 10 times molar excess of n-butyl lithium to one equivalent of CF-$LiFeTiO_4$. This resulted in an instant color change for all three reactions, from the salmon colored precursor CF-$LiFeTiO_4$ to a black powder. PXD of the 5 and 10 times excess products indicated the decomposition of CF-$LiFeTiO_4$ with no observable peaks and only an amorphous background. ICP analyses of the reaction products gave similar results with Li:Fe ratios of about 3.5:1 indicating almost complete reduction to Fe^{2+} and Ti^{2+}. After the addition of a molar ratio of n-butyl lithium to CF-$LiFeTiO_4$, observable peaks of CF-$LiFeTiO_4$ were present with a significant loss in intensities and an increase in background similar to those seen in the completely decomposed and amorphous 5 and 10 times excess n-butyl lithium reactions. These results can be explained by the large particle size of the precursor CF-$LiFeTiO_4$. The highly reactive nature of n-butyl lithium over-reduced the outside of the particles resulting in the decomposition and observed amorphous background while the centers of the particles were unreacted, explaining the presence of amorphous product as well as crystalline CF-$LiFeTiO_4$ in the PXD pattern. The observed decomposition of CF-$LiFeTiO_4$ on Li^+ intercalation at these experimental conditions was reported by us earlier [41].

Successful intercalation was achieved upon the slow (over 1 h) drop wise addition of diluted (0.1 molar) n-butyl lithium into a round bottom flask with 100 mL pentane and CF-$LiFeTiO_4$ in a N_2 glovebox. Due to the pyrophoric nature of the resulting compound the PXD measurements were taken on a Bruker D2 Phaser in a N_2 filled glovebox (Fig. 2(c)). All peaks in the PXD pattern can be indexed in an orthorhombic unit cell indicating single-phase product, as was later confirmed by structural refinement (see below). The cationic stoichiometry of the final product was $Li_{1.98(3)}Fe_{1.00}TiO_4$ as established by ICP analysis.

3.5. Chemical lithium deintercalation

Oxidation via chemical lithium deintercalation was performed by the addition of bromine and iodine solutions to CF-$LiFeTiO_4$. The reactions lead to product stoichiometries of $Li_{0.33(5)}Fe_{1.00}TiO_4$ and $Li_{0.55(5)}Fe_{1.00}TiO_4$ for reactions with bromine and iodine respectively. Considering that I_2/I^- and Br_2/Br^- redox couples have potentials of 3.5 and 4.1 V vs. Li [42], and that Fe^{4+}/Fe^{3+} redox potential is generally accepted to have substantially higher value, the low Li contents in the deintercalation products were unexpected. PXD patterns contained peaks of the initial CF-$LiFeTiO_4$ phase as well as an additional background due to an amorphous product. Earlier Fe^{4+} formation at these conditions was assumed based on PXD and ICP results [41]. However, further investigation with Mössbauer spectroscopy determined that Li deintercalation resulted in the decomposition of CF-$LiFeTiO_4$ without Fe^{4+} formation (see below).

3.6. Rietveld refinement of CF-$LiFeTiO_4$ crystal structure

The $NaFeTiO_4$ structure model was used as a starting point for the CF-$LiFeTiO_4$ refinement. The Rietveld refinement profiles of CF-$LiFeTiO_4$ PXD data are shown in Fig. 5(a), crystallographic data for CF-$LiFeTiO_4$ can be seen in Table 1, and the CF-$LiFeTiO_4$ structure is shown in Fig. 1(a). No attempts were made to refine Li in a less symmetrical position due to the low Li scattering power. Additional structural investigation might be needed to determine details of Li position. However, the structural motif of the parent compound was definitely preserved during the ion exchange. The space group Pnma was maintained from the precursor. The unit cell volume decreased by 3.1% for CF-$LiFeTiO_4$ in comparison with the precursor $NaFeTiO_4$ phase.

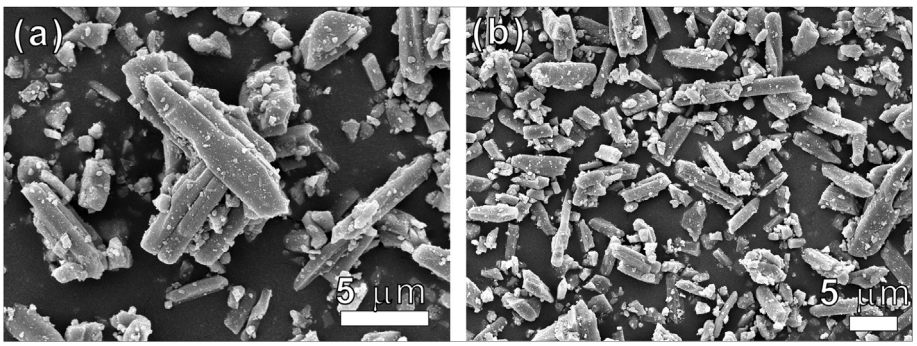

Fig. 4. SEM images of CF-$LiFeTiO_4$ illustrating the particles size of the compound in the multiple micrometer regime. The secondary electrons mode was used to obtain images.

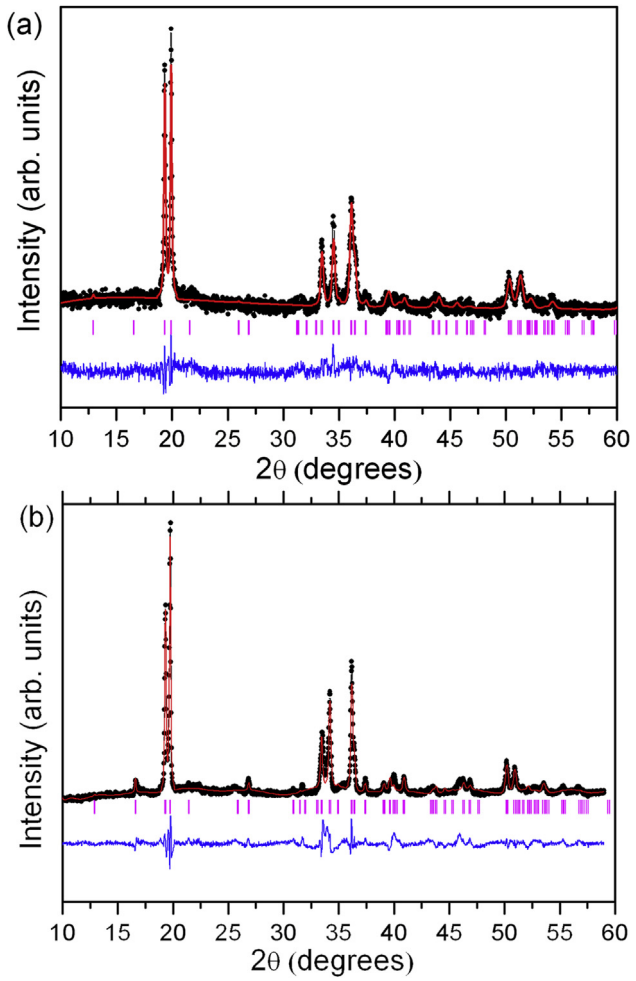

Fig. 5. Rietveld refinement profiles for the PXD data of (a) CF-$LiFeTiO_4$ and (b) CF-Li_2FeTiO_4: observed intensities (black circles), calculated pattern (red solid line), difference curve (blue bottom solid line), and Bragg positions (tick marks). (For interpretation of the references to color in this figure legend, the reader is referred to the web version of this article.)

3.7. Rietveld refinement of the CF-Li_2FeTiO_4 crystal structure

The crystal structure for Li_2FeTiO_4 was refined using CF-$LiFeTiO_4$ as an initial model with a second Li position added. The space group Pmna was maintained from the precursor. The Rietveld refinement profiles of the CF-Li_2FeTiO_4 are shown in Fig. 5(b), the CF-Li_2FeTiO_4 crystal structure is shown in Fig. 1(b) and crystallographic data are presented in Table 2.

Table 1
Crystallographic data for the Rietveld refinement of $LiFeTiO_4$[a].

Atom	Wyckoff position	*x*	*y*	*z*	10^2 U_{iso}(Å^2)	Occupancy
Li	4c	0.3409(5)	1/4	0.3498(5)	1.09(4)	1.
Fe1	4c	0.0774(3)	1/4	0.6344(5)	1.00(3)	0.5
Fe2	4c	0.0725(5)	1/4	0.1313(5)	0.99(6)	0.5
Ti1	4c	0.0774(3)	1/4	0.6344(5)	1.03(3)	0.5
Ti2	4c	0.0727(4)	1/4	0.1313(5)	0.99(5)	0.5
O1	4c	0.8945(6)	1/4	0.5201(1)	1.03(3)	1.
O2	4c	0.9996(3)	1/4	0.2875(3)	1.02(8)	1.
O3	4c	0.3079(2)	1/4	0.6299(8)	1.06(7)	1.
O4	4c	0.0676(1)	1/4	0.9434(2)	1.12(5)	1.

[a] Space group: Pnma (No. 62); $a = 8.9206(5)$ Å, $b = 2.9595(3)$ Å, $c = 10.710(1)$ Å.; $R_{wp} = 4.4\%$.

Table 2
Crystallographic data for the Rietveld refinement of Li_2FeTiO_4[a].

Atom	Wyckoff position	*x*	*y*	*z*	10^2 U_{iso}(Å^2)	Occupancy
Li	4c	0.3733(7)	1/4	0.3540(6)	0.96(2)	1
Li	4c	0.1146(9)	1/4	0.3124(1)	1.15(2)	1
Fe1	4c	0.0869(3)	1/4	0.6095(3)	1.07(3)	0.5
Fe2	4c	0.0684(3)	1/4	0.1161(3)	1.00(5)	0.5
Ti1	4c	0.0869(3)	1/4	0.6095(3)	1.09(2)	0.5
Ti2	4c	0.0684(3)	1/4	0.1161(3)	1.00(6)	0.5
O1	4c	0.8982(1)	1/4	0.5221(1)	0.98(5)	1
O2	4c	0.9528(1)	1/4	0.2728(1)	1.13(7)	1
O3	4c	0.3216(9)	1/4	0.6590(1)	1.00(4)	1
O4	4c	0.0830(1)	1/4	0.9215(1)	1.11(7)	1

[a] Space group: Pnma (No. 62); $a = 9.0525(3)$ Å, $b = 2.9566(2)$ Å, $c = 10.758(1)$ Å; $R_{wp} = 5.5\%$.

It is clear form the comparison of CF-$LiFeTiO_4$ and Li_2FeTiO_4 crystal structure (Fig. 1a and b) that Li intercalation occurred in a topotactic manner. The unit cell volume is 1.8% larger for Li_2FeTiO_4 due to Li incorporation in the structure. Strictly speaking, due to the presence of an additional Li cation the structure does not belong to the $CaFe_2O_4$-type. However, since the FeO_6 octahedra connectivity pattern is identical to that in $CaFe_2O_4$-type structures and to further emphasize the structural relation to the parent CF-$LiFeTiO_4$ phase, we have chosen to assign Li_2FeTiO_4 to $CaFe_2O_4$-type structures in this article.

3.8. Mössbauer spectroscopy

Mössbauer spectroscopy was performed on CF-$LiFeTiO_4$ and lithium deintercalated sample with the "$Li_{0.33}FeTiO_4$" average stoichiometry. The parameters extracted from the spectra fits are isomer shift, δ, quadrupole splitting, ΔE_Q, and peak areas.

The CF-$LiFeTiO_4$ spectrum contains a doublet, which can be fit with one Fe site (Fig. 6(a)). The δ value is in the typical range for Fe^{3+} (HS) in octahedral coordination (Table 3). The quadrupole splitting, leading to a doublet formation, is a result of a non-zero electric field gradient (EFG) at Fe nucleus. The two possible sources of EFG, valence electron contribution and lattice contribution, both would be equal to zero if FeO_6 octahedra had O_h symmetry. Thus, the presence of the quadrupole splitting indicates distortion of FeO_6 octahedra, which is in agreement with the refined crystal structure.

The spectrum of chemically deintercalated sample with an average stoichiometry "$Li_{0.33}FeTiO_4$" was fit with two Fe sites (Fig. 6(b)). One of the Fe sites has a δ value similar to that for Fe in CF-$LiFeTiO_4$; therefore, we attribute this doublet to Fe^{3+} (HS, octahedral) in CF-$LiFeTiO_4$ structure with some Li deintercalated. Another Fe site has slightly lower δ value (0.30 mm s^{-1}), nevertheless the δ value is still within values typical for Fe^{3+} ions. At the same time, the δ and ΔE_Q value combination does not allow assigning uniquely tetrahedral or octahedral coordination environment to this Fe site. This Fe site is most probably present in the amorphous decomposition product, which manifests itself as an increase in background in the PXD pattern. One can conclude that Li deintercalation did not lead to Fe^{4+} formation but to a decomposition product. Based on the average "$Li_{0.33}FeTiO_4$" stoichiometry and purely Fe^{3+} oxidation state, an oxygen loss can be assumed in the crystalline and amorphous products.

3.9. Electrochemical tests

Cyclic voltammetry at high potential range did not reveal any features before reaction with electrolytes. On the other hand, electrochemical cycling of CF-$LiFeTiO_4$ between 1.5 and 3.0 V at C/5

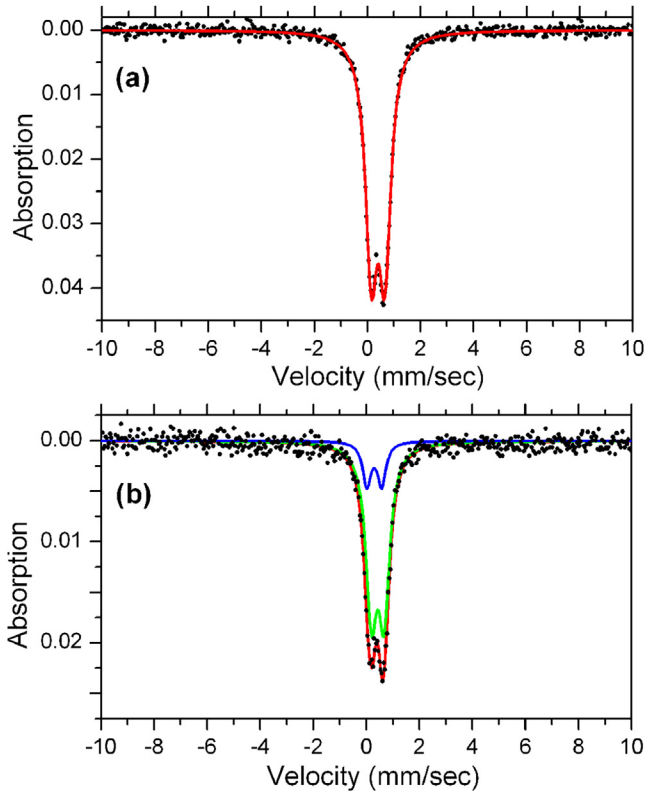

Fig. 6. Fits (red lines) of room temperature ^{57}Fe Mössbauer spectra of (a) CF-LiFeTiO$_4$ and (b) lithium deintercalated "Li$_{0.33}$FeTiO$_4$". In the "Li$_{0.33}$FeTiO$_4$" spectrum contributions from separate Fe sites is shown as green and blue lines. (For interpretation of the references to color in this figure legend, the reader is referred to the web version of this article.)

Table 3
Parameters from Mössbauer spectra fits of CF-LiFeTiO$_4$ and lithium deintercalated "Li$_{0.33}$FeTiO$_4$" product.

Compound	Isomer shift ± 0.02 (mm s^{-1})	Quadrupole splitting ± 0.02 (mm s^{-1})	Area ± 2 (%)
CF-LiFeTiO$_4$	0.40	0.51	100
"Li$_{0.33}$FeTiO$_4$"	0.43	0.48	83
	0.30	0.56	17

rate (Fig. 7(a)) showed deintercalation at about 2.3 V with gravimetric capacity of 148 mAh g^{-1}, which is very close to the theoretical value of 153 mAh g^{-1} for 1 Li intercalation. Severe cathode material polarization can be concluded by comparing the deintercalation and the intercalation potential values of 2.3 V and 2.0 V (Fig. 7(a)) and from charge–discharge curves (Fig. 7(b)). Low area of electrochemically active surface of crystallites is a possible cause for the polarization observed (see below). Continued cycling at this rate resulted in a capacity fade of 8% over ten cycles (Fig. 7(c)). Increasing the rate to C/2.5 for 50 cycles had a similar fade trend with a decreased starting capacity of about 121 mAh g^{-1} and a final capacity of 99 mAh g^{-1} a capacity fade of 18% over the 50 cycles. In the cycling rate of C/2.5, an initial capacity fade of about 1% occurs after each subsequent cycle and eventually decreases to less than 0.5%.

The slope of charge/discharge curves (Fig. 7(b)) indicates one phase electrochemical process, i.e. CF-LiFeTiO$_4$ and CF-Li$_2$FeTiO$_4$ do not separate in different regions but form a solid solution with an intermediate Li content.

Additional investigations are needed for detailed understanding of CF-LiFeTiO$_4$ electrochemical properties. Such detailed electrochemical study is beyond the scope of the article and will be published separately.

3.10. *Crystal structure–property relationships for spinel and tunnel LiFeTiO$_4$ polymorphs*

The CF-LiFeTiO$_4$ polymorph was prepared to test two fundamental crystal chemical ideas:

(1) the possibility of Fe^{4+} formation by Li$^+$ deintercalation and
(2) the ability of a structure with large tunnels prepared by an ion exchange to accommodate additional Li$^+$ ions.

Fe^{4+} formation was disproved by Mössbauer spectroscopy of chemically Li deintercalated samples. However, the intercalation of an additional Li$^+$ while preserving the structure motif was demonstrated by PXD and ICP. This confirms the initial hypothesis that the tunnels of this structure could harbor more lithium.

Comparing the crystal structures of the spinel and calcium ferrate type LiFeTiO$_4$ polymorphs (Fig. 1(a) and (c)), one has to consider Li and Fe mixing in the spinel structure. As determined by powder neutron diffraction (PND), in spinel LiFeTiO$_4$ the cationic distribution corresponds to $(Li_{0.47}Fe_{0.53})_A(Li_{0.53}Fe_{0.47}Ti)_BO_4$ where *A* and *B* denote the tetrahedral and octahedral sites respectively [35,43]. The Li/Fe mixing impedes Li$^+$ diffusion and results in a high, 0.9 eV, diffusion activation energy [35]. On the contrary, no Li/Fe mixing was reported for the precursor NaFeTiO$_4$ [44] used as the precursor for the preparation of CF-LiFeTiO$_4$ in this article. It was assumed and later confirmed by Rietveld refinement that low temperature ion exchange would preserves the initial structure and would not lead to Li/Fe position sharing in CF-LiFeTiO$_4$.

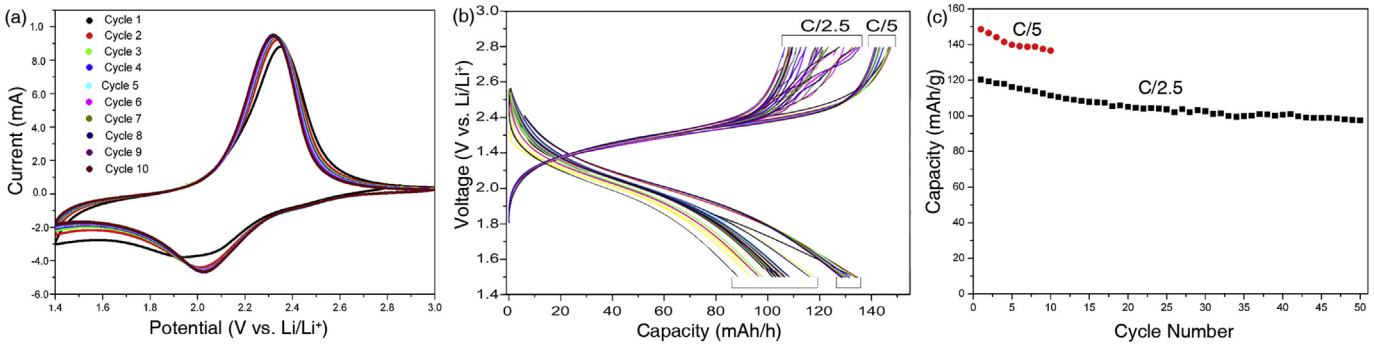

Fig. 7. Electrochemical characterization of CF-LiFeTiO$_4$ cycled against Li metal (a) cyclic voltammogram between 1.4 V and 3.0 V measured at C/5 rate, (b) the integrated CV (charge–discharge) curves measured at rate of C/5 and C/2.5 and (c) CF-LiFeTiO$_4$ specific capacity as a function of number of charge–discharge cycles.

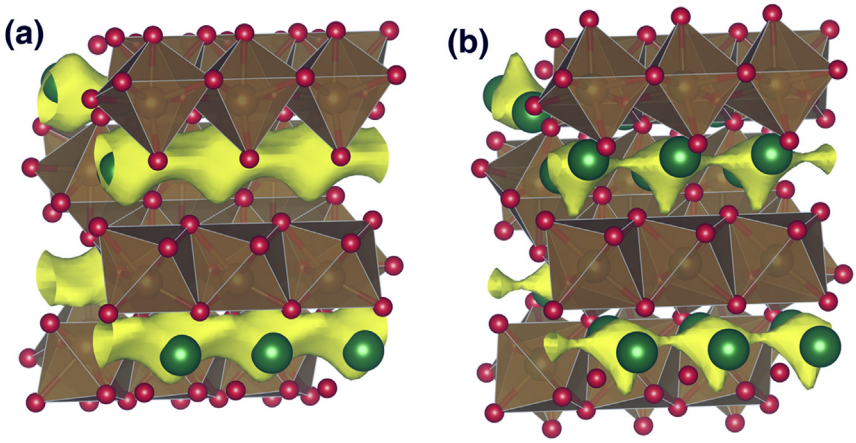

Fig. 8. Li^+ bond valence sum isosurfaces (yellow) at BVS values of 1.0 for (a) CF-$LiFeTiO_4$ and (b) CF-Li_2FeTiO_4. Atom color scheme is the same as in Fig. 1. (For interpretation of the references to color in this figure legend, the reader is referred to the web version of this article.)

To visualize the possible Li^+ diffusion paths, bond valence sum (BVS) maps were calculated for CF-$LiFeTiO_4$ and CF-Li_2FeTiO_4 (Fig. 8). As seen in Fig. 8, the isosurfaces with BVS for Li^+ equal to one are already interconnected for both compounds. Thus, the diffusion can be expected to have a small activation energy, which should result in fast ionic diffusion. It is known that crystallite growth occurs fastest in the direction of the smallest unit cell parameter; therefore, the rod-like CF-$LiFeTiO_4$ particles (Fig. 4) can be expected to have the long direction coinciding with the *b* unit cell parameter, i.e. coinciding with the structural tunnels and easy Li^+ diffusion direction in the crystal structure. Therefore, Li^+ intercalation/deintercalation most probably occurs only at the tips of the rod-like crystals where tunnels are exposed to the electrolyte. The length of the CF-$LiFeTiO_4$ crystal in the middle of Fig. 4(a) is ~17 μm. It is impressive that in spite of low surface area available for Li^+ intercalation (just the crystal tips) reasonable cycling rates can be supported (Fig. 7). This observation is in agreement with fast Li^+ diffusion expected from BVS maps.

Synthesis of nanosized particles and carbon coating was required for electrochemical cycling of rock-salt Li_2FeTiO_4 polymorph [36]. Fast cycling between CF-$LiFeTiO_4$ and CF-Li_2FeTiO_4 compounds was achieved without any cathode optimization.

4. Conclusions

New polymorphs CF-$LiFeTiO_4$ and CF-Li_2FeTiO_4 were successfully synthesized. Li deintercalation from CF-$LiFeTiO_4$ resulted in compound decomposition without Fe^{4+} formation. However, CF-Li_2FeTiO_4 formation supports the hypothesis that an extra Li^+ can be topotactically intercalated in a tunnel structure provided that tunnels are sufficiently large. Thus, investigation of complex 3*d* metal oxides with large tunnels can potentially lead to a discovery of a compound with 2 redox couples, M^{2+}/M^{3+} and M^{3+}/M^{4+}, accessible for utilization during electrochemical cycling, i.e. to discovery of a high energy density cathode with multiple electrons transfer per transition metal.

Acknowledgments

This work was supported by the National Science Foundation through Grant DMR-1206718. We thank Matthew Dyer from the University of Liverpool for the development of BVS-Mapping software. The Mössbauer lab at the Advanced Photon Source is partially supported by COMPRES (the Consortium for Materials Properties Research in Earth Sciences).

References

[1] J.B. Goodenough, Y. Kim, Chem. Mater. 22 (2010) 587–603.
[2] B.L. Ellis, K.T. Lee, L.F. Nazar, Chem. Mater. 22 (2010) 691–714.
[3] A.K. Padhi, K.S. Nanjundaswamy, J.B. Goodenough, J. Electrochem. Soc. 144 (1997) 1188–1194.
[4] M.M. Thackeray, W.I.F. David, J.B. Goodenough, Mater. Res. Bull. 17 (1982) 785–793.
[5] S. Komaba, T. Mikumo, N. Yabuuchi, A. Ogata, H. Yoshida, Y. Yamada, J. Electrochem. Soc. 157 (2010) A60–A65.
[6] G. Jain, M. Balasubramanian, J.J. Xu, Chem. Mater. 18 (2006) 423–434.
[7] H. Morimoto, S. Tobishima, Y. Iizuka, J. Power Sources 146 (2005) 315–318.
[8] X.L. Wu, Y.G. Guo, L.J. Wan, C.W. Hu, J. Phys. Chem. C 112 (2008) 16824–16829.
[9] M. Hibino, J. Terashima, T. Yao, J. Electrochem. Soc. 154 (2007) A1107–A1111.
[10] D. Larcher, C. Masquelier, D. Bonnin, Y. Chabre, V. Masson, J.B. Leriche, J.M. Tarascon, J. Electrochem. Soc. 150 (2003) A133–A139.
[11] P. Gibot, M. Casas-Cabanas, L. Laffont, S. Levasseur, P. Carlach, S. Hamelet, J.M. Tarascon, C. Masquelier, Nat. Mater. 7 (2008) 741–747.
[12] C. Delmas, M. Maccario, L. Croguennec, F. Le Cras, F. Weill, Nat. Mater. 7 (2008) 665–671.
[13] S. Nishimura, G. Kobayashi, K. Ohoyama, R. Kanno, M. Yashima, A. Yamada, Nat. Mater. 7 (2008) 707–711.
[14] K. Amine, H. Yasuda, M. Yamachi, J. Power Sources 82 (1999) 221–223.
[15] R. Kanno, T. Shirane, Y. Kawamoto, Y. Takeda, M. Takano, M. Ohashi, Y. Yamaguchi, J. Electrochem. Soc. 143 (1996) 2435–2442.
[16] C. Benoit, C. Bourbon, P. Berthet, S. Franger, J. Phys. Chem. Solids 67 (2006) 1265–1269.
[17] F. Zhou, X. Zhao, C. Yuan, H. Xu, Chem. Lett. 35 (2006) 1410–1411.
[18] S.-H. Wu, H.-Y. Liu, J. Power Sources 174 (2007) 789–794.
[19] K. Kanamura, H. Sakaebe, Z.-i. Takehara, J. Power Sources 40 (1992) 291–298.
[20] Z.-i. Takehara, H. Sakaebe, K. Kanamura, J. Power Sources 44 (1993) 627–634.
[21] T. Matsumura, R. Kanno, Y. Inaba, Y. Kawamoto, M. Takano, J. Electrochem. Soc. 149 (2002) A1509–A1513.
[22] R. Kanno, T. Shirane, Y. Inaba, Y. Kawamoto, J. Power Sources 68 (1997) 145–152.
[23] A.R. Armstrong, D.W. Tee, F. La Mantia, P. Novak, P.G. Bruce, J. Am. Chem. Soc. 130 (2008) 3554–3559.
[24] J.L.C. Rowsell, J. Gaubicher, L.F. Nazar, J. Power Sources 97–98 (2001) 254–257.
[25] X.X. Shi, C.X. Chang, J.F. Xiang, Y. Xiao, L.J. Yuan, J.T. Sun, J. Solid State Chem. 181 (2008) 2231–2236.
[26] Y.Z. Dong, Y.M. Zhao, Z.D. Shi, X.N. An, P. Fu, L. Chen, Electrochim. Acta 53 (2008) 2339–2345.
[27] V. Legagneur, Y. An, A. Mosbah, R. Portal, A.L. La Salle, A. Verbaere, D. Guyomard, Y. Piffard, Solid State Ionics 139 (2001) 37–46.
[28] N. Recham, J.N. Chotard, L. Dupont, C. Delacourt, W. Walker, M. Armand, J.M. Tarascon, Nat. Mater. 9 (2010) 68–74.
[29] B.L. Ellis, W.R.M. Makahnouk, Y. Makimura, K. Toghill, L.F. Nazar, Nat. Mater. 6 (2007) 749–753.
[30] A. Nyten, S. Kamali, L. Haggstrom, T. Gustafsson, J.O. Thomas, J. Mater. Chem. 16 (2006) 2266–2272.
[31] T. Ohzuku, K. Ariyoshi, S. Takeda, Y. Sakai, Electrochim. Acta 46 (2001) 2327–2336.

[32] J. Zhao, L.W. Zhao, N. Dimov, S. Okada, T. Nishida, J. Electrochem. Soc. 160 (2013) A3077–A3081.
[33] D.P. Lv, J.Y. Bai, P. Zhang, S.Q. Wu, Y.X. Li, W. Wen, Z. Jiang, J.X. Mi, Z.Z. Zhu, Y. Yang, Chem. Mater. 25 (2013) 2014–2020.
[34] D.P. Lv, W. Wen, X.K. Huang, J.Y. Bai, J.X. Mi, S.Q. Wu, Y. Yang, J. Mater. Chem. 21 (2011) 9506–9512.
[35] M.A. Arillo, M.L. Lopez, E. Perez-Cappe, C. Pico, M.L. Veiga, Solid State Ionics 107 (1998) 307–312.
[36] M. Kuzma, R. Dominko, A. Meden, D. Makovec, M. Bele, J. Jamnik, M. Gaberscek, J. Power Sources 189 (2009) 81–88.
[37] A.C. Larson, R.B. Von Dreele, Los Alamos National Laboratory Report LAUR, vol. 86, Los Alamos National Laboratory, Los Alamos, NM, 2000, p. 748.
[38] B.H. Toby, J. Appl. Crystallogr. 34 (2001) 210–213.
[39] K. Momma, F. Izumi, J. Appl. Crystallogr. 44 (2011) 1272–1276.
[40] M.B.M. Jari Hjollum, http://arxiv.org/abs/0912.0449, 2009.
[41] S.R. Bruno, C.K. Blakely, C.M. Tenbusch, V.V. Poltavets, ECS Trans. 45 (2013) 23–28.
[42] A.R. Wizansky, P.E. Rauch, F.J. Disalvo, J. Solid State Chem. 81 (1989) 203–207.
[43] M.A. Arillo, M.L. Lopez, C. Pico, M.L. Veiga, J. Campo, J.L. Martinez, A. Santrich-Badal, Chem. Mater. 17 (2005) 4162–4167.
[44] H. Muller-Buschbaum, D. Frerichs, J. Alloy Compd. 199 (1993) L5–L8.